

# Highly Sensitive H<sub>2</sub>S Sensing with Gold and Platinum Surface Modified ZnO Nanowire ChemFETs

Angelika Kaiser <sup>1,\*</sup>, Erick Torres Ceja <sup>1</sup>, Florian Huber <sup>1</sup>, Ulrich Herr <sup>2</sup> and Klaus Thonke <sup>1</sup>

<sup>1</sup> Institute of Quantum Matter/Semiconductor Physics Group, Ulm University, Germany; erick.torres-ceja@uni-ulm.de (E.T.C.); florian.huber@alumni.uni-ulm.de (F.H.); klaus.thonke@uni-ulm.de (K.T.)

<sup>2</sup> Institute of Functional Nanosystems, Ulm University, Germany; ulrich.herr@uni-ulm.de

\* Correspondence: angelika.kaiser@uni-ulm.de; Tel.: +49-(0731)-50-26132

Received: date; Accepted: date; Published: date

**Abstract:** In this work, we investigate the catalytic effects of gold (Au) and platinum (Pt) nanoparticle layer deposition on highly sensitive zinc oxide (ZnO) nanowires (NW) used for selective H<sub>2</sub>S detection in the sub-ppm region. Optimum quality pristine ZnO NWs are grown by high temperature chemical vapor deposition (CVD) in the vapor liquid solid growth (VLS) mode on silicon with a thin Au layer acting as a growth catalyst. The surface of pristine ZnO NWs was modified by systematic magnetron sputtering of discontinuous Au and Pt layers of 0 – 5 nm thickness. Resistive gas sensors based on the gas sensing mechanism of a chemical field effect transistor (ChemFET) with open gate, which is formed by hundreds of parallel aligned pristine, Au modified or Pt modified ZnO NWs, were measured towards H<sub>2</sub>S diluted in dry nitrogen (N<sub>2</sub>) or in dry synthetic air at room temperature. Gas sensing results show a largely improved response due to the catalytic effects of metal deposition on ZnO NW surface. Controlled application of ZnO NW growth under optimized conditions and metal catalyst deposition shows a clear response enhancement towards 1 ppm H<sub>2</sub>S from initial 20% achieved with pristine ZnO to over 5000% with ZnO NWs covered by 5 nm of Au, and hence significantly lower the limit of detection.

**Keywords:** ZnO; H<sub>2</sub>S; Au; Pt; Catalyst; ChemFET; Gas Sensor; eNose

---

## 1. Introduction

Over the past decade, numerous publications highlighted the medical role of hydrogen sulfide (H<sub>2</sub>S) for therapeutic applications and early diagnostics [1,2], traced in medical breath analysis e.g., with the “electronic nose” approach [3]. It was shown that abnormal endogenous H<sub>2</sub>S concentration levels in exhaled breath samples can be linked to airway inflammation in asthma patients, and hence H<sub>2</sub>S functions as a potent biomarker.

Expired human breath is mainly consisting of nitrogen, oxygen, and carbon dioxide, in addition to numerous volatile organic compounds (VCO) and sulfides (such as H<sub>2</sub>S) in the low ppt - ppb concentration range. Using ion-molecule reaction-mass spectrometry, Milloning et al. successfully linked an exhaled trace amount of 1.9 ppb of H<sub>2</sub>S to gastroesophageal cancer [4]. Zhang et al. studied eosinophilic asthma and paucigranulocytic asthma in 97 patients. In their studies, both chronic asthma types showed correlation to exhaled endogenous H<sub>2</sub>S concentrations of 7.7 ppb and 11.1 ppb, respectively [5]. A fast and selective detection of such small concentrations is challenging. Here, standard sensing procedures are often using mass spectrometry, gas chromatograph or IR gas sensors [6–8]. Despite offering a reliable and selective detection technique, the instruments for these sensing approaches are bulky and expensive [7]. Moreover, breath sample preparation and analysis rely on

big volume samples or the conversion of H<sub>2</sub>S before detection [9], which appears to be difficult when used for real medical breath detection with patients.

A less expensive and simple sensing approach is based on the cost-effective production and application of nano scaled metal oxides [10], which are used for integrated chemiresistive gas sensor arrays of electronic nose (e-Nose) sensing systems. Here, a vast variety of metal oxides for H<sub>2</sub>S detection was investigated, including WO<sub>3</sub> [11], CuO [12], SnO<sub>2</sub> [13],  $\alpha$ -Fe<sub>2</sub>O<sub>3</sub> [14] and ZnO [15]. Wu et al. presented a gas sensor based on  $\alpha$ -Fe<sub>2</sub>O<sub>3</sub> nano ellipsoids synthesized through hydrothermal method with reliable sensing response towards 1 – 400 ppm of H<sub>2</sub>S and an excellent detection limit of 100 ppb at 350 °C [16]. A fast and significant response towards 50 ppb of H<sub>2</sub>S at room temperature was achieved by Wang et al. with a gas sensor based on hydrothermal ZnO nanorods [17].

The fabrication of highly selective room temperature gas sensors with enhanced gas sensing mechanics often require the combination of several metal oxides, additional doping or metal oxide surface modification with catalytic noble metals such as Au and Pt [18,19]. Sharma et al. demonstrated how gold modified ZnO nanoplates showed an enhanced response towards H<sub>2</sub>S [20] and Zhou et al. reached detection limit of even 25 ppb for H<sub>2</sub>S detection with well-dispersed Pt nanoparticles on a complex ZnO structure [21]. These studies present a promising material platform for highly sensitive H<sub>2</sub>S detection.

The main aim of our work is the successful detection of H<sub>2</sub>S trace amounts in the low ppb concentration range at room temperature. Therefore, we analyze and compare resistive gas sensors based on pristine high quality ZnO NWs grown by high temperature CVD with ZnO NWs after systematic surface modification with the noble metals Au and Pt. Resistive gas sensors based ZnO with nanoparticle layers ranging from 0 - 5 nm of catalyst thickness are investigated towards sensor response, signal-to-noise ratio and limit of detection. We show that Au/ZnO NW gas sensors are superior in comparison to gas sensors based on pristine ZnO NWs and Pt/ZnO NWs and allow for H<sub>2</sub>S detection in synthetic air at room temperature with an estimated limit of detection of 7 ppb.

## 2. Materials and Methods

### 2.1. ZnO Nanowire Growth

ZnO NWs were grown by high temperature CVD using VLS growth [22] in a movable three zone tube furnace with a horizontal quartz glass liner tube. The upstream side of the quartz glass liner tube has a gas inlet for argon (Ar, 99.998% purity, 190 sccm flow rate). The downstream side has a gas inlet for oxygen (O<sub>2</sub>, 99.995% purity diluted in Ar down to 5%, 1.14 sccm flow rate) and is also connected to a vacuum pump. For the growth 300 mg source material were used, which consists of carbon powder and ZnO powder (99.99% purity) in the molar ratio 1:1. As substrate silicon (100) wafer pieces of 1 cm<sup>2</sup> total size with a 3 nm thick gold layer on top were used, the latter acting as a catalyst for the NW growth. The source material was placed upstream inside the three zone furnace at a temperature of 1045 °C. The substrate was placed 25 cm downstream from the source material at a temperature of 1057 °C. The oxygen inlet was 1 cm upstream next to the substrate. Growth took place at stabilized tube pressure of 900 mbar. During the 60 min long growth process evaporated ZnO was reduced to Zn vapour, which was transported by the argon carrier gas towards the oxygen inlet and substrate. Here the Zn reoxidized to ZnO within the catalytic Au/Zn alloy droplets on the Si substrate surface. These droplets act as nucleation sites for the ZnO NW growth. After successful growth, we obtained a dense nanowire forest of approximately 40 µm long and 100 nm thick ZnO NWs as shown in Figure 1a.

A detailed study about the ZnO NW growth process was reported in our previous work by Li et al. and Huber et al. [23,24].

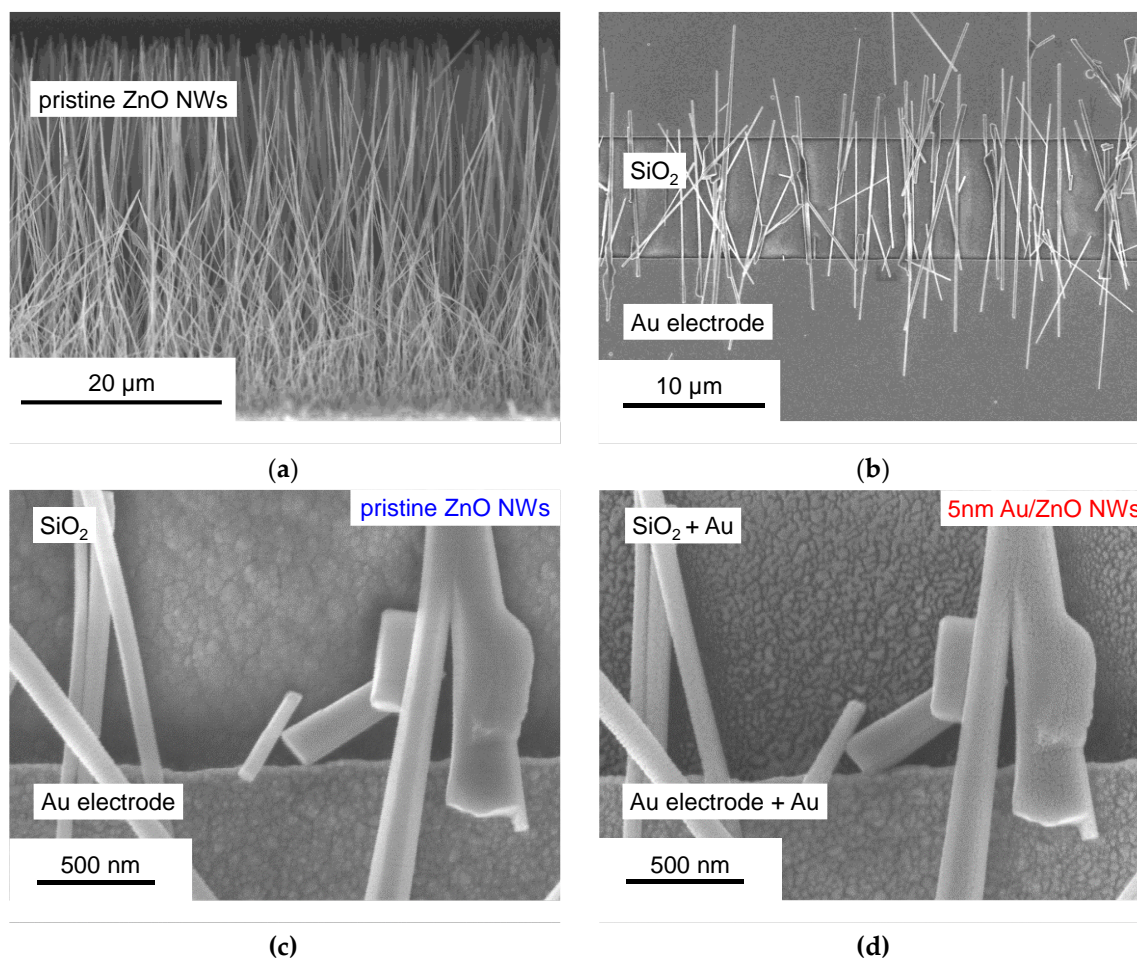


**Figure 1.** Scanning electron micrographs of (a) pristine ZnO NWs as grown on Si with Au catalyst and (b) after deposition via dielectrophoresis between two parallel Au contact pads on the sensor surface; (c,d) ZnO NWs before and after surface modification with 5 nm of Au by room temperature magnetron sputtering. The deposited metal catalyst forms a discontinuous nanoparticle layer.

## 2.2. Gas sensor fabrication and metal surface modification of ZnO nanowires

Sensors were fabricated from hundreds of ZnO NWs bridging the 5–10  $\mu\text{m}$  gap between two Ti/Au contact stripes on a silicon substrate with 900 nm insulating  $\text{SiO}_2$  on top (Figure 1b). In a first step, the ZnO NWs were harvested from the growth substrate with an ultrasonification bath while being diluted in 1000  $\mu\text{L}$  of isopropanol. In a second step, 40  $\mu\text{L}$  of this solution were drop coated onto a single contact structure and aligned by dielectrophoresis [25]. For a reproducible and homogeneous surface modification of the ZnO NW sensors, Au and Pt were deposited by magnetron sputtering. Here, a Bal-Tec Med 020 high vacuum coating system was used. The investigated nanoparticle layer thicknesses ranged from 0–5 nm. A nanoparticle layer thickness higher than 5–7 nm leads to a shortcut, and hence prohibited sensing via the ZnO NWs [26]. The sputtering values for Au and Pt deposition at room temperature were  $5 \cdot 10^{-2}$  Pa base pressure and  $7 \cdot 10^{-3}$  Pa sputtering pressure, a sputtering power of 7 W; and a target size of 2". After 90 s a uniform Au film of 5 nm could be achieved. During the sputtering process the film thickness was monitored via a quartz crystal microbalance placed next to the sensor samples. This microbalance was calibrated for Au and Pt magnetron sputtering by X-ray reflectometry (XRR) measurements using test samples. Figure 1c,d shows the sensor surface before and after surface modification with 5 nm Au nanoparticle layer thickness. During surface modification metal nanoparticle islands are formed and created a discontinuous film. A thicker nanoparticle catalyst loading will close the gaps between the islands and lead to a continuous and conducting layer, hence leading to the unwanted shortcut between the contact pads of the sensor.

### 2.3. Measurement Setup and Gas Sensor Evaluation

A schematic representation of our gas sensing setup is displayed in Figure 2a with the measurement chamber encircled in red. The chamber was a circular stainless-steel gas compartment with a small total gas volume of 11 mL (Figure 2c) and room for two sensors, which could be measured simultaneously. The chamber was temperature stabilized by a water bath. General gas testing measurements were executed at a stable room temperature of  $(20 \pm 1)^\circ\text{C}$  in dynamic flux measurements under a gas flow of 42 sccm/min. The tested gas atmosphere was pre-mixed and diluted in a computer controlled mixing stage, consisting of several mass flow controllers and one pressure controller. Gases used in our measurements were 1 ppm of H<sub>2</sub>S (98% purity) prediluted in nitrogen (N<sub>2</sub>, 99.9999% purity), which could be diluted further with nitrogen (N<sub>2</sub>, 99.9999% purity) or synthetic air (N<sub>2</sub>, 99.9999% purity with O<sub>2</sub>, 99.995% purity mixed in a N<sub>2</sub>:O<sub>2</sub> ratio of 4:1), pure nitrogen (N<sub>2</sub>, 99.9999% purity) and pure oxygen (O<sub>2</sub>, 99.995% purity). Each selected atmosphere was tested in generally 10 min long intervals, alternating between the testing gas atmosphere and a flushing gas atmosphere in a series of multiple detection cycles. For the electrical evaluation of the gas measurement response, we applied 1 V to every sensor (Figure 2b) and acquired the current flow  $I$  through the ZnO NWs over the time  $t$  with a combination of switchable low-noise transimpedance amplifiers and a 12 bit analog-digital converter (ADC). Data were recorded with an acquisition rate of  $1/s$ . As a result a  $I(t)$  trace was measured and further investigated by the estimation of the reference current level  $I_0$  (or quiescent current level) in a neutral flushing gas interval, which was acquired for each sensor by flushing the samples with pure N<sub>2</sub>, O<sub>2</sub> or synthetic air for a minimum of 10 min before introducing desired target gas to the sensor. Based on the reference current level the response was defined as [27]:

$$R(\%) = (I_g - I_0)/I_0 \cdot 100, \quad (1)$$

where  $I_g$  is the measured current level through the ZnO NWs at the end of a target gas. The sensitivity is defined as the slope of the response  $\Delta R$  over the detected target gas concentration  $\Delta c$ :

$$S = \frac{\Delta R}{\Delta c}, \quad (2)$$

which is needed in order to estimate the theoretical **LOD** value via the given definition [28]:

$$LOD = 3 \frac{RMS}{S}. \quad (3)$$

where, **RMS** stands for the root mean square noise of the response  $R$  and is further used to estimate the signal-to-noise ratio:

$$SNR = \frac{RMS}{R}, \quad (4)$$

of our sensors.

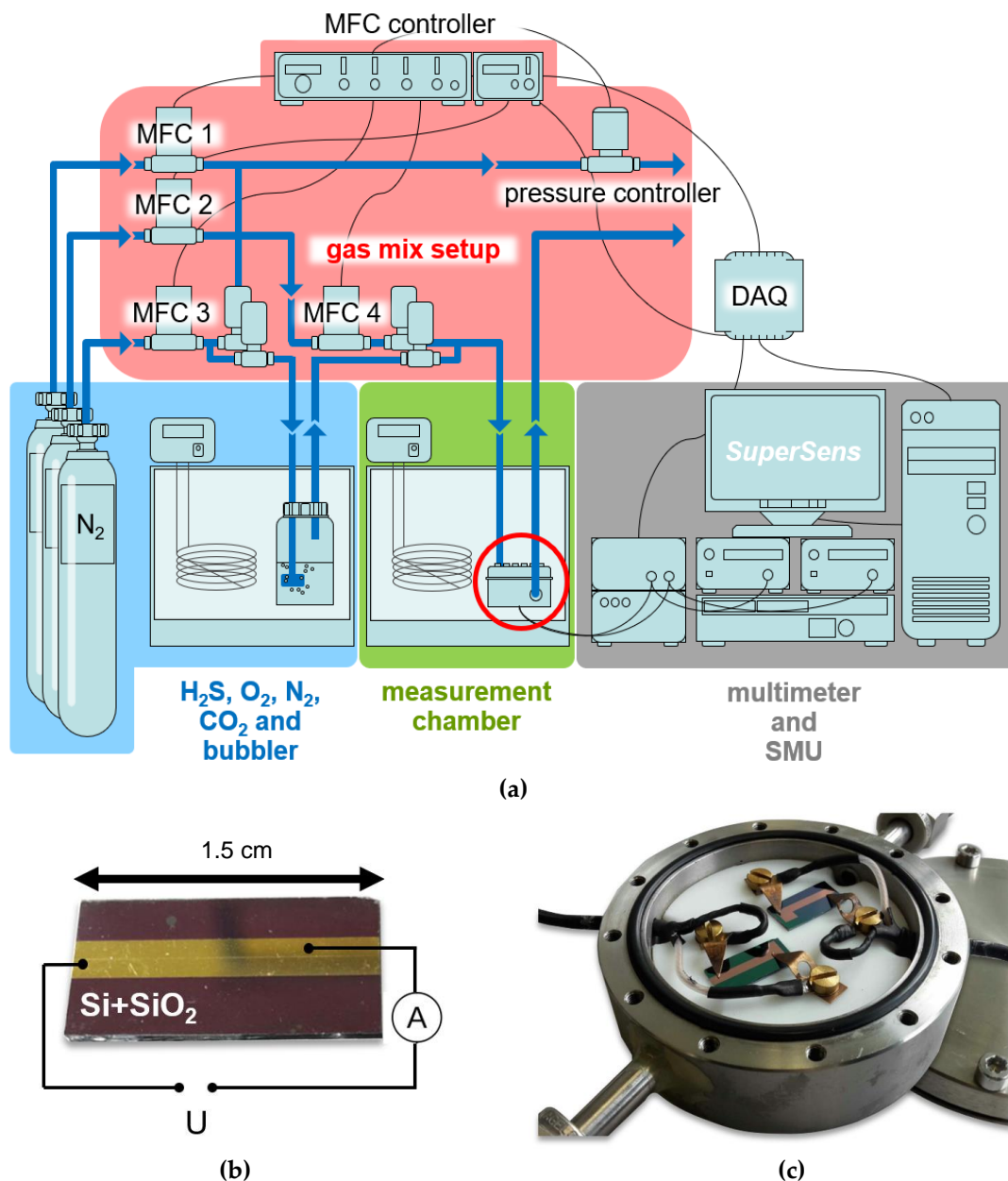


**Figure 2.** Schematic overview of core components of the measurement setup: (a) gas sensing setup with computer controlled mixing stage, multiple high purity gases, temperature stabilized measurement chamber encircled in red and data acquisition; (b) planar sensor with two 1.5 cm long parallel Au electrodes on Si with insulating SiO<sub>2</sub>; (c) sealed stainless steel measurement chamber with a total gas compartment of 11 mL and two gas sensors mounted.

### 3. Results

#### 3.1. Gas Sensing with Pristine, Au Modified and Pt Modified ZnO Nanowires

The main aim of this work is to achieve a first and detailed understanding of the effects of surface modification of ZnO NWs with metal catalysts, here especially Au and Pt, on gaseous H<sub>2</sub>S detection. The detection of H<sub>2</sub>S with sensors using initially pristine ZnO NWs was compared to H<sub>2</sub>S detection results of the same sensors after metal catalyst deposition. In order to separate the role of both metal catalysts from the general sensing attributes of ZnO, the sensor characteristics, e.g., the response  $R$  towards 1 ppm of H<sub>2</sub>S, sensitivity  $S$  and  $LOD$ , were evaluated and compared between samples with pristine and surface modified ZnO NWs of the same CVD growth batch.

For the first measurement series two sensors, loaded with pristine ZnO NWs from the same growth run, were fabricated. The  $I(V)$ -curves of both sensors are displayed in Figure 3 and showed a comparable current level of  $7.2 \mu\text{A}$  and  $8.9 \mu\text{A}$  at  $1\text{V}$  respectively. After electrical comparison of both sensors, they were tested in a first gas sensing measurement. The surrounding atmosphere for both sensors was periodically switched between pure  $\text{O}_2$  and  $1 \text{ ppm}$  of  $\text{H}_2\text{S}$  diluted in  $\text{N}_2$ , starting with  $\text{O}_2$  as the flushing gas interval and  $\text{H}_2\text{S}$  diluted in  $\text{N}_2$  as the target gas interval. The  $R(t)$ -data for sensor 1 and sensor 2 are shown in Figure 4a. The response of the ZnO NWs towards  $\text{H}_2\text{S}$  appears to be hardly visible and reaches  $R = (20 \pm 15)\%$  for sensor 2 when considering the noise level. Since the  $\text{SNR}$  for both sensors with pristine ZnO NWs appeared was close to 2, and hence the noise is very high in comparison to the detection signal, an estimation of the response for both sensors was difficult.

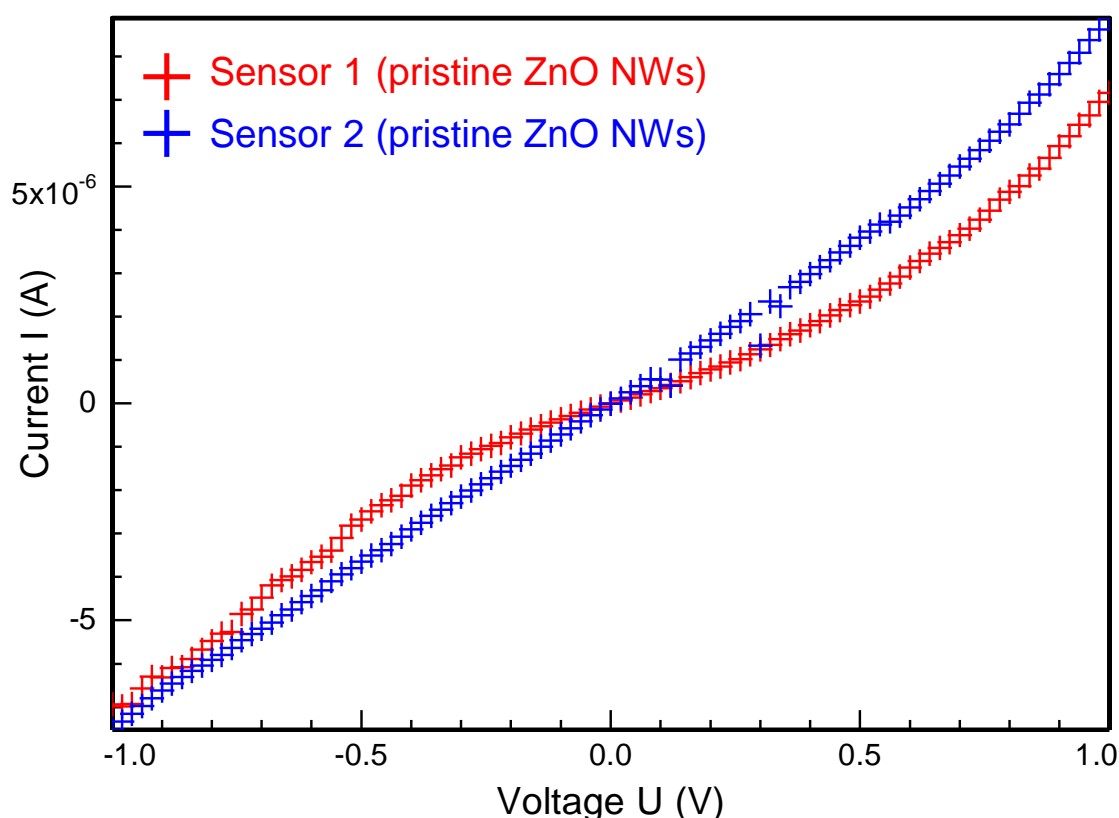


**Figure 3.** Nonlinear and symmetric  $I(V)$ -curve of two nominally identical sensors with pristine ZnO NWs fabricated from the same growth sample.

In the next step,  $5 \text{ nm}$  Au was deposited on sensor 2 and  $\text{H}_2\text{S}$  sensing measurements were performed with sensor 1 and sensor 2 again. In Figure 4b the  $R(t)$ -data for sensor 1 and sensor 2 after the modification of sensor 2 are displayed. The modified sensor 2 reached a response of  $R = (5480 \pm 15)\%$  towards  $1 \text{ ppm}$   $\text{H}_2\text{S}$  in the first detection cycle. As expected, the signal of sensor 1 stayed noisy with a response  $R$  below  $100\%$ . This tremendous increase of response towards  $1 \text{ ppm}$  of  $\text{H}_2\text{S}$  with Au modified ZnO NWs in comparison to pristine ZnO NWs clearly demonstrates the beneficial effect of Au modification for  $\text{H}_2\text{S}$  detection with ZnO NWs. A closer look into the  $R(t)$ -data of sensor 2 after the modification revealed that the enhancement of the sensors response due to the

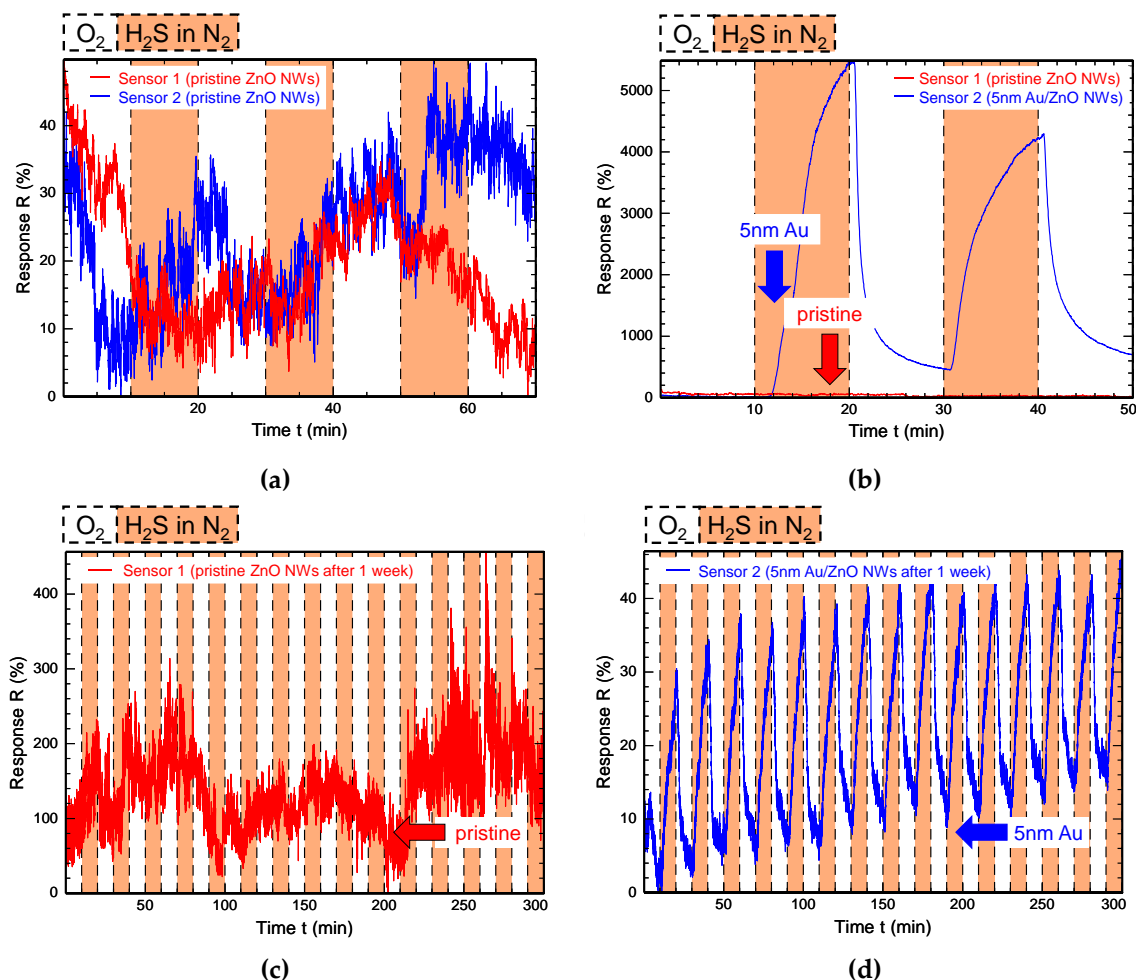


**Figure 4.** Comparison of H<sub>2</sub>S detection results of pristine or Au surface modified ZnO NWs. (a)  $R(t)$ -data of sensors 1 and sensor 2 before surface modification reaching a response of  $R = (20 \pm 15)\%$  towards 1 ppm target gas concentration; (b) after 5 nm Au deposition on sensor 2 the response towards 1 ppm H<sub>2</sub>S is drastically increased to  $R = (5480 \pm 15)\%$ ; (c) after 1 week of continuous measurement sensor 1 showed a high noise level and no clear response towards 1 ppm H<sub>2</sub>S; (d) after 1 week only the surface modified sensor 2 still responds towards H<sub>2</sub>S. Due to ongoing contamination of the Au catalyst the enhanced response decreased to a stable value of  $R = (25 \pm 5)\%$ .

Au catalyst decreased over time, because the response in the second detection cycle in Figure 4b only reached  $R = (3840 \pm 15)\%$ . Continuous testing of sensor 1 and sensor 2 for one week after modification revealed a strong decay of the sensors response (Figure 4c,d). After one week of measurement the response of sensor 2 towards 1 ppm of H<sub>2</sub>S decreased but also stabilized at  $R = (25 \pm 5)\%$  with an improved *SNR* of 5 in comparison to the equivalent measurement with ZnO NWs without modification. After one week of measurements no clear response could be acquired for the pristine ZnO NWs of sensor 1 due to the high noise level.

In the second measurement series surface modification of ZnO NWs with Pt or Au was compared. Two sensors were fabricated from the same ZnO NW growth run by dropping 40  $\mu$ L pristine ZnO NW solution onto two 1.5 cm long contact structures. After successful dielectrophoresis alignment sensor 1 was modified with 5 nm Au, and sensor 2 with 3 nm Pt. Any higher Pt loading has lead to a shortcut, as mentioned in Section 2.2, and hence wasn't considered for comparison. Both sensors were tested at room temperature in a total of 13 detection cycles by periodically switching between the flushing gas atmosphere of pure O<sub>2</sub> and the testing gas atmosphere of 1 ppm H<sub>2</sub>S diluted in N<sub>2</sub>. Figure 5a,b displays the measured  $I(t)$ -data of both sensors. Due to the visible upwards drift for both sensors, the corresponding response for each detection cycle are displayed separately in Figure 5c. Comparing the  $I(t)$ -data of 5 nm Au/ZnO NWs with 3 nm Pt/ZnO NWs reveals a better

SNR after Pt modification than after Au modification, what can be attributed to a unaffected noise level despite an increased reference current level. The response was enhanced for both sensors and reached a peak response of  $R = (570 \pm 40)\%$  for sensor 1 with Au modification in comparison to a peak response of  $R = (40 \pm 1)\%$  for sensor 2 with Pt modification. A decrease in response towards 1 ppm H<sub>2</sub>S with ongoing measurement cycles was observed for both sensors. For the Au modified sensor the peak response decreased by a factor of 3 down to a stable response of  $R = (190 \pm 40)\%$ , whereas the already lower peak response of the Pt modified sensor decreased by a factor of 13 down to a stable response of  $R = (3 \pm 1)\%$ . Both sensors, especially the Pt modified ZnO NWs, showed an upwards drift of the reference current level. This is most likely caused by a catalytically assisted accumulation of H<sub>2</sub>S on the ZnO NW surface in the testing gas interval, which is leading to a desorption reaction of O<sub>2</sub>, in comparison to the less likely O<sub>2</sub> adsorption which should be taking place in the flushing gas interval. This drift will be discussed in Section 4 in closer detail.

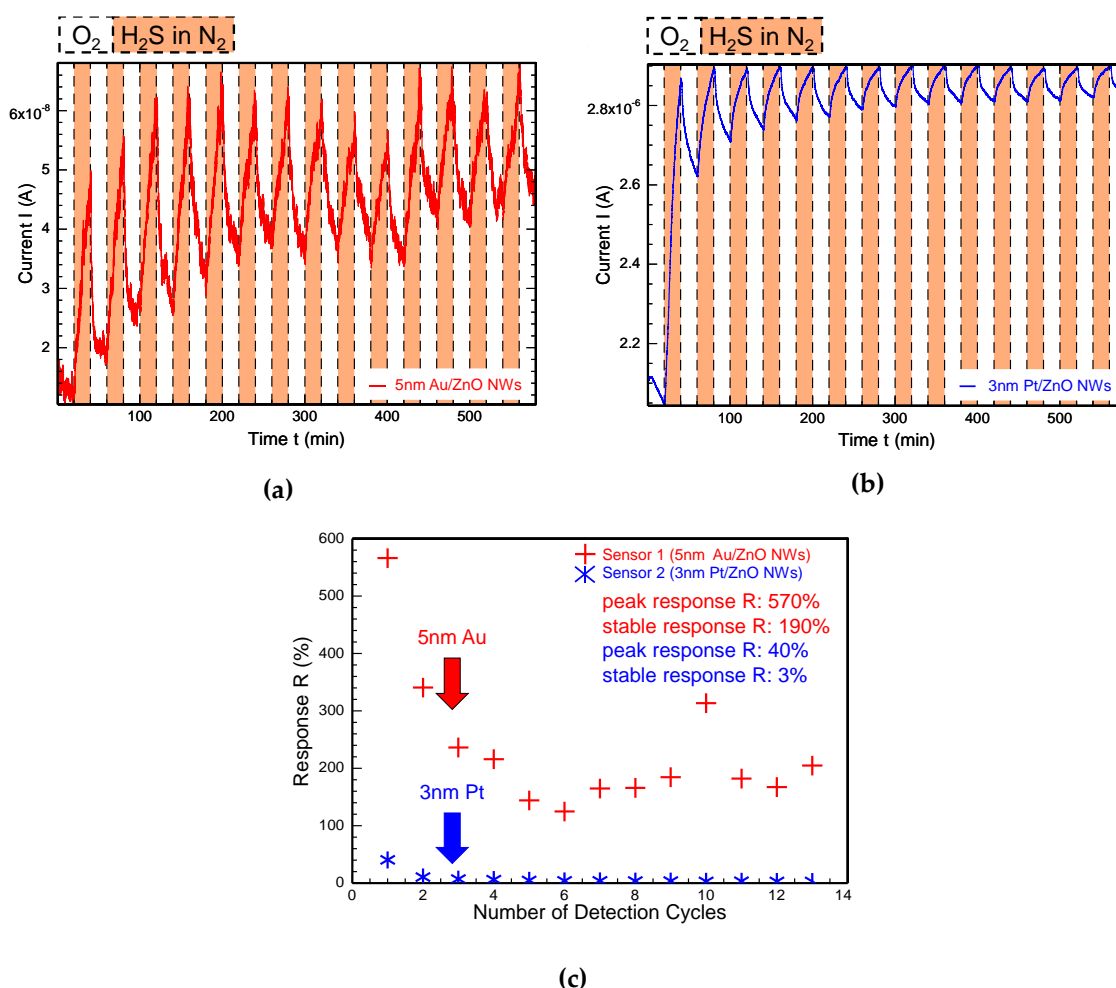


**Figure 5.** Comparison of H<sub>2</sub>S detection results of Au and Pt surface modified ZnO NWs. (a,b)  $I(t)$ -data of sensors 1 and sensor 2 after surface modification with 5 nm Au and 3 nm Pt towards 1 ppm H<sub>2</sub>S respectively; (c) equivalent response data for both sensors collected for 13 continuous measurement cycles. The response towards H<sub>2</sub>S with Au modified ZnO NWs appears to be superior with a peak response of  $R = (570 \pm 40)\%$  in comparison to a peak response of  $R = (40 \pm 1)\%$  with Pt modified ZnO NWs. Both sensors show a continuously decreasing H<sub>2</sub>S response due to a contamination of the metal catalyst caused by ongoing H<sub>2</sub>S exposure.

Overall, our comparison of pristine, Au modified and Pt modified ZnO NWs demonstrates that Au is a reliable and more stable catalyst for H<sub>2</sub>S detection with ZnO NWs than Pt.



### 3.3. Systematic Au Surface Modification of ZnO NWs

So far, we verified Au as a stable and promising catalyst candidate for gaseous H<sub>2</sub>S detection with ZnO NWs. For a more detailed understanding of the catalytical effects of Au modification on ZnO NW surface further investigation regarding a dependance between response enhancement and Au nanoparticle layer thickness and a closer look into the stability of the Au modification over time has been done.

Therefore, a new sensor with initially pristine NWs was manufactured and tested for 1 ppm H<sub>2</sub>S detection in 10 min long testing gas intervals. After the first recorded gas measurement results, the sensor was modified with a 1 nm thick Au nanoparticle layer and then tested for 1 ppm H<sub>2</sub>S detection again. This increase of Au loading in steps of 1 nm on a single sensor and the corresponding evaluation was continued until the final Au nanoparticle layer thickness of 5 nm was deposited. Hence,  $R(t)$ -data for 1 ppm H<sub>2</sub>S detection with pristine ZnO NWs and ZnO NWs with 1 nm, 2 nm, 3 nm, 4 nm and 5 nm Au catalyst loading on a single sensor was acquired and is displayed in Figure 6 and Table 1. The total measurement duration took 4 days.

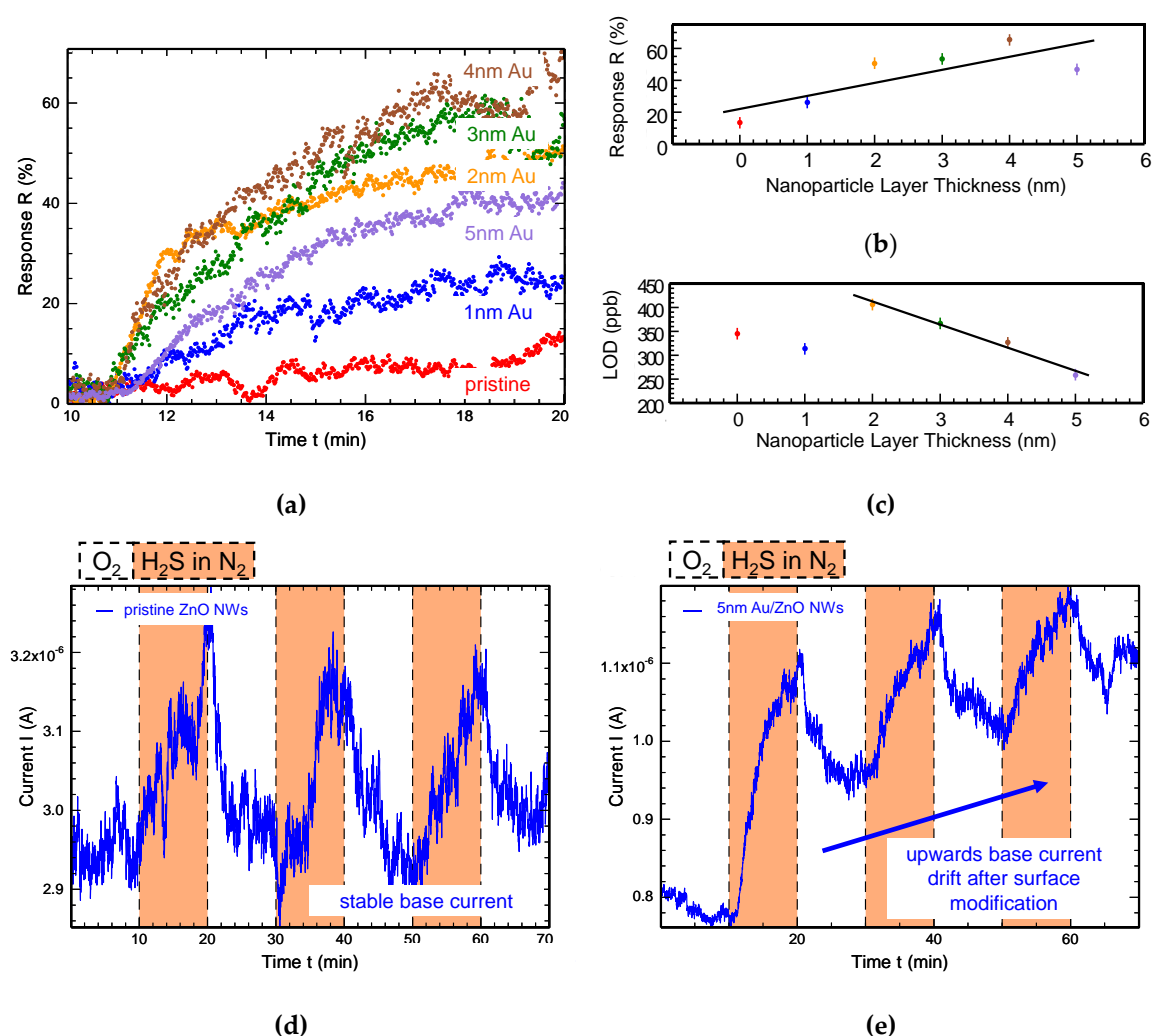


**Figure 6.** H<sub>2</sub>S detection results for stepwise Au modified ZnO NWs: (a)  $R(t)$ -data towards 1ppm H<sub>2</sub>S for pristine ZnO NWs in the first target gas interval, and ZnO NWs modified by 1 nm, 2 nm, 3 nm, 4 nm and 5 nm for the same sensor. (b,c) With increasing Au catalyst loading the response increased from initial  $R = (13 \pm 5)\%$  with pristine ZnO NWs up to  $R = (65 \pm 5)\%$  with 4 nm Au/ZnO NWs. The  $LOD$  decreases with stepwise Au modification in an apparently linear tendency, which is displayed a black curve. (d,e) Direct comparison of raw  $I(t)$ -data before and after surface modification

of sensor 1. After the modification with Au sensors show an upwards base current drift as a result of favored detection of H<sub>2</sub>S in comparison to O<sub>2</sub> adsorption.

The sensor with pristine ZnO NWs reached a response of  $R = (13 \pm 5)\%$  for 1 ppm H<sub>2</sub>S. This response continuously increased until the sensor reached a response of  $R = (65 \pm 5)\%$  towards 1 ppm H<sub>2</sub>S with 4 nm Au/ZnO NWs. For 5 nm Au catalyst loading the response decreased. The *RMS* for the measurements appeared to be independent from the Au nanoparticle layer thickness. As displayed in Figure 6b the response towards 1 ppm H<sub>2</sub>S was increasing with a thicker Au catalyst layer and the *LOD* was decreasing from  $(405 \pm 40)$  ppb down to  $(259 \pm 40)$  ppb (Figure 6c) with a continuously improved initial *SNR* = 9 with pristine ZnO NWs to *SNR* = 12 with 5 nm Au/ZnO loading.

This measurement series revealed a continuous improvement of several gas sensor characteristics like response *R*, *SNR* and *LOD* with increasing catalyst loading. It is very likely that a decreasing sensor response in spite of an increasing catalyst layer thickness is attributed to the decay of the catalyst itself during 4 days of continuous measurements. This decay was already observed in Section 3.1 and appeared after a first introduction of H<sub>2</sub>S towards the sensors. The response towards H<sub>2</sub>S with the 5 nm Au/ZnO NWs in this measurement series appeared to be lower than in the previous results, which were discussed in Section 3.2. This is also very much a consequence of the ongoing decay of the catalyst.

Figure 6d and Figure 6e display a direct comparison of the raw *I(t)*-data of sensor 1 towards the detection of 1 ppm H<sub>2</sub>S before and after the completed surface modification of the ZnO NWs. It is clearly visible how the base current level showed drifting behavior only after the nanowire modification, what will be discussed in chapter 4 in more detail.

**Table 1.** H<sub>2</sub>S response results and *LOD* for stepwise Au modified ZnO NWs.

Sensor	Response <i>R</i> (%)	<i>LOD</i> (ppb)
pristine ZnO NWs	$(13 \pm 5)$	$(345 \pm 40)$
1 nm Au/ZnO NWs	$(26 \pm 5)$	$(313 \pm 40)$
2 nm Au/ZnO NWs	$(51 \pm 5)$	$(405 \pm 40)$
3 nm Au/ZnO NWs	$(53 \pm 5)$	$(366 \pm 40)$
4 nm Au/ZnO NWs	$(65 \pm 5)$	$(326 \pm 40)$
5 nm Au/ZnO NWs	$(47 \pm 5)$	$(259 \pm 40)$

#### 3.4. *LOD* towards H<sub>2</sub>S Detection in Synthetic Air with Pristine and Surface Modified ZnO NWs

So far, we investigated the detection of H<sub>2</sub>S diluted in N<sub>2</sub> to low ppm concentrations. For a first attempt on medical breath analysis with pristine and surface modified ZnO NWs an investigation of H<sub>2</sub>S detection in the ppb range is of great interest. In order to model a first basic breath sample, H<sub>2</sub>S needs to be diluted in dry synthetic air.

Therefore, two more sensors from the same ZnO NWs growth sample were processed, and their gas sensing abilities were tested towards low ppb-concentrations of H<sub>2</sub>S diluted in dry synthetic air. Sensor 1 was fabricated from pristine ZnO NWs, and sensor 2 was using nominally identical pristine ZnO NWs with additional surface modification with a 5 nm Au layer. Both sensors were tested in sensing cycles of 20 min long flushing gas intervals and testing gas intervals. Flushing gas was dry synthetic air, and testing gas was 60–180 ppb of H<sub>2</sub>S diluted in dry synthetic air. Additional 30 min intervals of pure O<sub>2</sub> in between different H<sub>2</sub>S concentrations made sure that both sensors experienced different concentrations at comparable starting conditions.

The results of this measurement are displayed in Figure 7. Figure 7a shows the *R(t)*-data for both sensors. Sensor 1 with pristine ZnO NWs showed no response towards 60 ppb, 120 ppb or 180 ppb of H<sub>2</sub>S diluted in dry synthetic air. The surface modified sensor 2 showed a clear response of  $R = (250 \pm 60)\%$  towards 60 ppb of H<sub>2</sub>S. This response increased to  $R = (780 \pm 60)\%$  for the detection of 180 ppb of H<sub>2</sub>S. As displayed in Figure 7b the detection data of sensor 2 showed a clear

linear dependence between response  $R$  and the detected concentration  $c$ . With a sensitivity of  $S = (4400 \pm 300) \text{ ppm}^{-1}$  and a  $RMS$  of 10 this led to a theoretically estimated  $LOD$  of  $(7 \pm 5) \text{ ppb}$  for the detection of  $\text{H}_2\text{S}$  diluted in dry synthetic air at room temperature. This experimentally and theoretically acquired  $LOD$  result for surface modified ZnO NWs in comparison to pristine ZnO NWs highlights the necessity and great potential of metal catalysts for  $\text{H}_2\text{S}$  detection with ZnO NWs. The selective detection of the resistive gas  $\text{H}_2\text{S}$  in the low ppb concentration range side by side to the strongly oxidative  $\text{O}_2$  is a cause of the strong chemical affinity between Au and S and is discussed in Section 4.

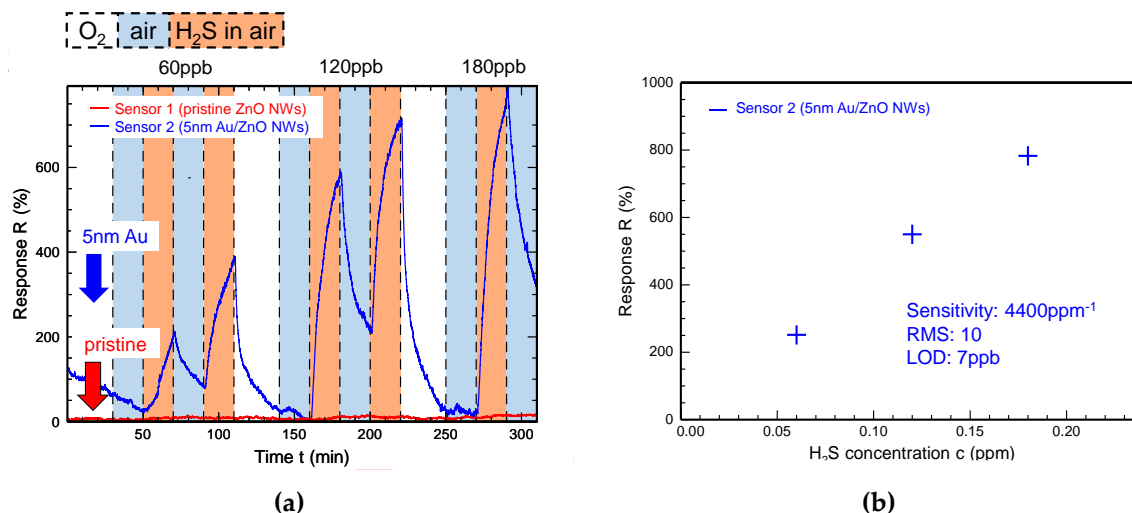
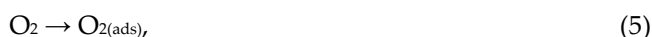


**Figure 7.** Detection results for  $\text{H}_2\text{S}$  diluted in synthetic air with pristine and Au modified ZnO NWs: (a) Pristine ZnO NWs showed no reaction towards 60 ppb of  $\text{H}_2\text{S}$  diluted in air while Au modified ZnO NWs enabled the detection of  $\text{H}_2\text{S}$  in the low ppb range. (b) A theoretical estimation of the sensor sensitivity towards  $\text{H}_2\text{S}$  in diluted air led to a  $LOD$  of 7 ppb.

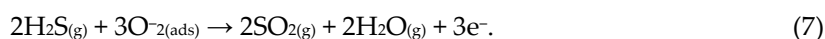
#### 4. Discussion

The gas-response mechanism of ZnO NWs is explained by adsorption and desorption reactions of reductive and oxidative gas molecules on a metal oxide surface. Nominally undoped ZnO typically is an n-type semiconductor due to surface and defect states such as oxygen vacancies. These additional states lead to the formation of a permanent non-conducting depletion layer at the ZnO NW surface and a remaining n-type conductive nanowire core.

When ZnO gets exposed to an oxidizing gas such as oxygen, these molecules ionosorb to active adsorption sites on the nanowire surface by trapping electrons from the n-type conducting core to themselves as shown in Figure 8a. This leads to an agglomeration of adsorbed anionic oxygen species, representing an additional negative charge, causing an upwards bending of the ZnO band structure at the nanowire reducing the diameter of conductive core. Thus, the resistance of the ZnO NWs increases and the current through the wires drops. At room temperature the adsorption process of the flushing gas  $\text{O}_2$  can be described as [29]:



If in turn a reducing gas, in our case the target gas  $\text{H}_2\text{S}$ , is brought in contact with the ZnO NWs, it reacts with the previously adsorbed oxygen species which leads to a desorption of the latter [30,31]:



The freed electrons are released back to the conducting nanowire core, and the surface band bending is reduced, i.e., the depletion region becomes thinner and the conducting core becomes wider, resulting in a higher current. This adsorption and desorption reaction of oxidative and

reductive gas is commonly observed for metal oxides, and specifically for pristine ZnO NWs specifically.

If a metal catalyst such as Au or Pt is introduced to a metal oxide surface, a series of possible effects are mentioned in literature, which will have a strong impact on the gas-response mechanism. A commonly reported effect for surface modification of metal oxides with Au and Pt is the formation of multiple nano-Schottky barriers at the contact region between the metal oxide and the metal catalyst (Figure 8b) [32]. The work function of Au and Pt [33] is larger than that of ZnO [34], which leads to a transfer of electrons from the nanowire core to the noble metal islands on the surface. These additional “nano-depletion regions” will be modulated by ongoing oxygen adsorption and desorption, leading to a greatly enhanced resistance and current change within the ZnO NWs and hence an enlarged response. This effect was easily confirmed by our measurements in the case of Au.

Another beneficial effect for gas detection with metal modified metal oxides, especially Au modified ZnO NWs, is the catalytically activated dissociation of H<sub>2</sub>S molecules on Au nanoparticle islands [35]. Due to a chemical affinity between Au and S, Au islands are active agglomeration sites for H<sub>2</sub>S molecules (Figure 8c). This agglomeration leads to a quantitatively increased interaction between H<sub>2</sub>S molecules and previously adsorbed O<sub>2</sub> molecules, which is supported by the improved *R* and *LOD* of our Au modified sensors.

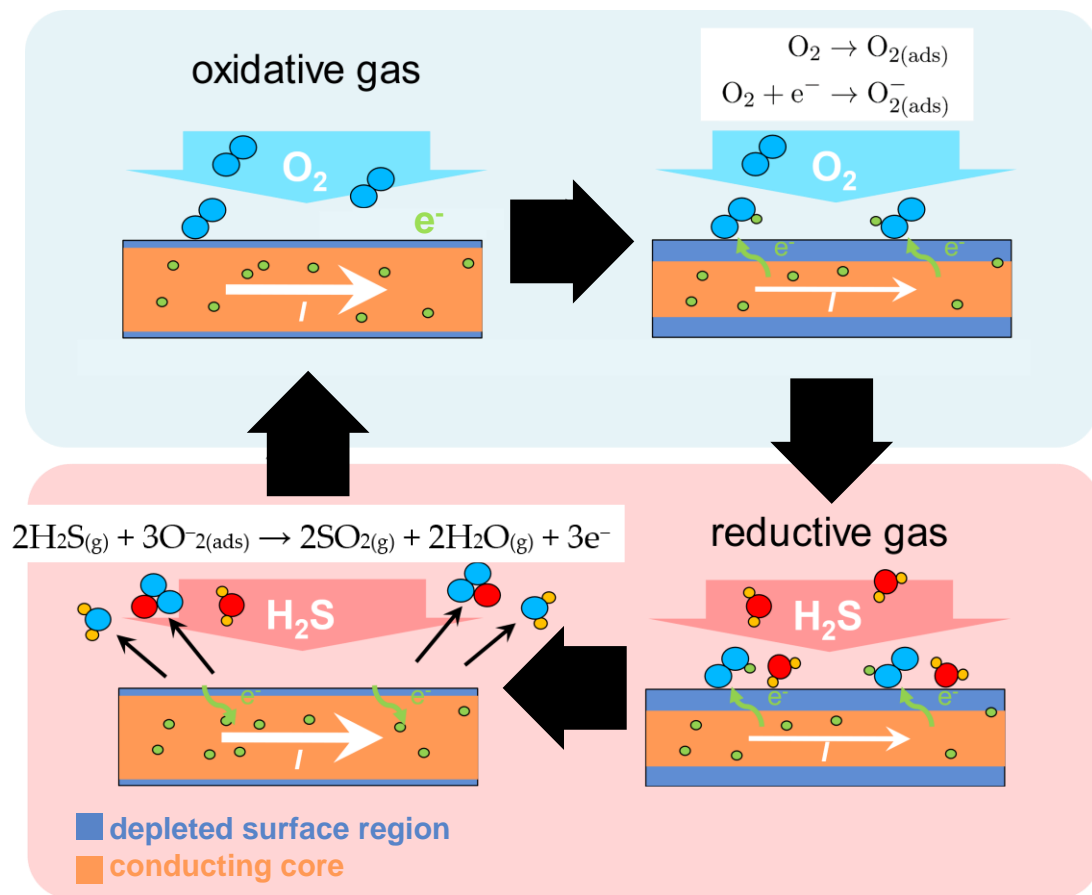
A similar effect is expected for the catalytic dissociation of oxygen at Au and Pt nanoparticle island [36,37]:



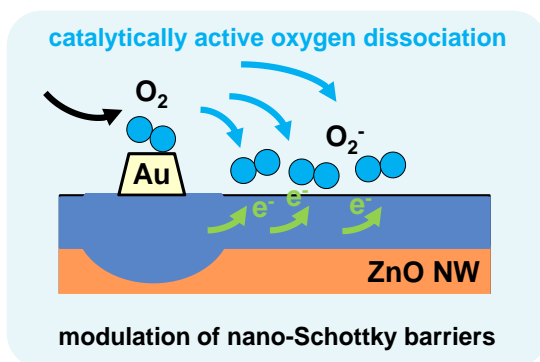
and [38]:



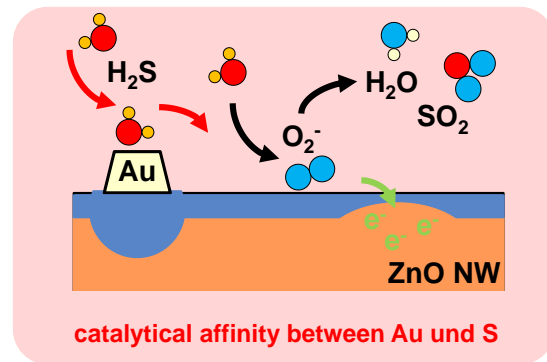
This catalytic ionization of O<sub>2</sub> should greatly enhance the adsorption reaction of O<sub>2</sub> and should result in a significantly decreased reference current level or a highly increased absorption rate for oxygen in our flushing gas intervals. However, our data do not support an enhanced dissociation of oxygen after surface modification of initially pristine ZnO NWs. A visible reference current drift after surface modification with said metal catalysts indicates a favoured H<sub>2</sub>S dissociation instead of an oxygen dissociation. This is further confirmed by the successful detection of H<sub>2</sub>S concentrations in the low ppb range in synthetic air. Here, 60 ppb of H<sub>2</sub>S could be detected in the presence of 15% highly of oxidative O<sub>2</sub>.



(a)



(b)



(c)

**Figure 8.** Gas-response mechanism of (a) pristine ZnO NWs; (b) Au and Pt modified ZnO NWs as well as (c) the catalytic affinity between Au modified ZnO NWs and S. Multiple additional nano-depletion regions on metal modified ZnO NWs lead to an enhanced response of the gas sensors. The affinity between Au and S leads to a selective detection of H<sub>2</sub>S with Au modified ZnO NWs and enables H<sub>2</sub>S detection in the low ppb concentration range.

While the catalytic dissociation of H<sub>2</sub>S due to driven by the Au surface modification led to a tremendous enhancement of the sensitivity of ZnO NWs, the strong affinity between Au and S may also be the reason for an ongoing and irreversible contamination of the catalyst as well. The strong chemical affinity between Au and S presumably led to a reactive interaction between both elements [32,39,40]:



H<sub>2</sub>S agglomerates at the Au islands and reacts to Au-SH and Au-S type species which results in a sulfurization of the Au catalyst over time [32]. Continuous exposure to H<sub>2</sub>S decreases the catalytic efficiency of Au modified ZnO NWs. This behaviour was observed for each sensor sample after Au surface modification, and needs further investigation in order to use Au/ZnO as a reliable sensing material for H<sub>2</sub>S detection in the low ppb concentration range.

## 5. Conclusions

H<sub>2</sub>S gas detection in the low ppb concentration range was successfully performed with pristine, Au modified and Pt modified ZnO NWs. The nanowires have been grown by high temperature CVD on Si (100) with a thin Au layer on top acting as growth catalyst. The as-grown ZnO NWs have been deposited via dielectrophoresis and functionalized with Au and Pt using magnetron sputtering at room temperature. Systematic comparison of H<sub>2</sub>S detection with pristine and modified nanowires of the same nanowire growth process was performed, including Pt catalyst loadings of 3 nm and Au catalyst loadings of 1 nm, 2 nm, 3 nm, 4 nm and 5 nm. Surface modification with Au led to a consistent enhancement of the gas sensing properties such as response *R*, *SNR* and *LOD*. While this was expected from literature for both Au and Pt modification, our measurements could only confirm the catalytically enhanced detection of H<sub>2</sub>S with Au surface modified ZnO NWs. The so far investigated modification method led to a large enhancement of the sensitivity, however this initial improvement was also decreasing with ongoing H<sub>2</sub>S exposure due to a degradation of the applied metal catalysts. This was most likely caused by a sulfurization process of the catalyst, which can be expected because of the strong chemical interaction between sulfur and Au. On the other hand, the same chemical interaction allowed for the detection of extremely low experimentally and theoretically estimated *LODs* of 60 ppb and 7 ppb of H<sub>2</sub>S diluted in synthetic air at room temperature and hence highlights Au/ZnO NWs as a very potent sensing material for biomarker detection in the low ppb concentration range.

## 6. Patents

**Author Contributions:** Conceptualization, A.K.; methodology, A.K., F.H., U.H. and K.T.; software, K.T.; validation, A.K., E.T.C., F.H., U.H. and K.T.; formal analysis, A.K. and E.T.C.; resources, U.H. and K.T.; data curation, A.K. and E.T.C.; writing—original draft preparation, A.K.; writing—review and editing, A.K., U.H. and K.T.; visualization, A.K.; supervision, U.H. and K.T.; project administration, U.H. and K.T. All authors have read and agreed to the published version of the manuscript.

**Funding:** We thank the “DFG-Deutsche Forschungsgemeinschaft” for funding this project under contract number 398819137.

**Acknowledgments and Funding:** The authors thank Dr. H. Schieferdecker for the dedicated technical support in the measurement setup.

## References

1. Wang, P.; Zhang, G.; Wondimu, T.; Ross, R.; Wang, R. Hydrogen sulfide and asthma. *Exp. Physiol.* **2011**, *96*, 847–852, doi:10.1113/expphysiol.2011.057448.
2. Szabó, C. Hydrogen sulphide and its therapeutic potential. *Nat. Rev. Drug. Discov.* **2007**, *6*, 917–935, doi:10.1038/nrd2425.
3. D’Amico, A.; Pennazza, G.; Santonico, M.; Martinelli, E.; Roscioni, C.; Galluccio, G.; Paolesse, R.; Di Natale, C. An investigation on electronic nose diagnosis of lung cancer. *Lung Cancer* **2010**, *68*, 170–176, doi:10.1016/j.lungcan.2009.11.003.
4. Millonig, G.; Praun, S.; Netzer, M. Non-invasive diagnosis of liver diseases by breath analysis using an optimized ion-molecule reaction-mass spectrometry approach: A pilot study. *Biomarkers* **2010**, *15*, 297–306, doi:10.3109/13547501003624512.

5. Zhang, J.; Wang, X.; Chen, Y.; Yao, W. Correlation between levels of exhaled hydrogen sulfide and airway inflammatory phenotype in patients with chronic persistent asthma. *Respirology* **2014**, *19*, 1165–1169, doi:10.1111/resp.12372.
6. Wondimu, T.; Wang, R.; Ross, B. Hydrogen sulphide in human nasal air quantified using thermal desorption and selected ion flow tube mass spectrometry. *J. Breath Res.* **2014**, *8*, 036002, doi:10.1088/1752-7155/8/3/036002.
7. Zampolli, S.; Elmi, I.; Mancarella, F.; Betti, P.; Dalcanale, E.; Cardinali, G.C.; Severi, M. Real-time monitoring of sub-ppb concentrations of aromatic volatiles with a MEMS-enabled miniaturized gas-chromatograph. *Sens. Actuators B: Chem.* **2009**, *141*, 322–328, doi:10.1016/j.snb.2009.06.021.
8. Petrucci, J.; Cardoso, A.A.; Wilk, A.; Kokoric, V.; Mizaikoff, B. iCONVERT: An Integrated Device for the UV-Assisted Determination of H<sub>2</sub>S via Mid-Infrared Gas Sensors. *Anal. Chem.* **2015**, *87*, 9580–9583, doi:10.1021/acs.analchem.5b02731.
9. Petrucci, J.; Cardoso, A.A.; Wilk, A.; Mizaikoff, B. Online Analysis of H<sub>2</sub>S and SO<sub>2</sub> via Advanced Mid-Infrared Gas Sensors. *Anal. Chem.* **2015**, *87*, 9605–9611, doi:10.1021/acs.analchem.5b02730.
10. Moon, H.G.; Jung, Y.; Han, S.D.; Shim, Y.; Shin, B.; Lee, T.; Kim, J.; Lee, S.; Jun, S.C.; Park, H.; et al. Chemiresistive Electronic Nose toward Detection of Biomarkers in Exhaled Breath. *ACS Appl. Mater. Interfaces* **2016**, *8*, 20969–20976, doi:10.1021/acsami.6b03256.
11. Ionescu, R.; Hoel, A.; Granqvist, C.G.; Llobet, E.; Heszler, P. Low-level detection of ethanol and H<sub>2</sub>S with temperature-modulated WO<sub>3</sub> nanoparticle gas sensors. *Sens. Actuators B: Chem.* **2005**, *104*, 132–139, doi:10.1016/j.snb.2004.05.015.
12. Zhang, D.; Wu, J.; Cao, Y. Ultrasensitive H<sub>2</sub>S gas detection at room temperature based on copper oxide/molybdenum disulfide nanocomposite with synergistic effect. *Sens. Actuators B: Chem.* **2019**, *287*, 346–355, doi:10.1016/j.snb.2019.02.008.
13. Choi, S.-J.; Jang, B.-H.; Lee, S.-J.; Min, B.K.; Rothschild, A.; Kim, I.-D. Selective Detection of Acetone and Hydrogen Sulfide for the Diagnosis of Diabetes and Halitosis Using SnO<sub>2</sub> Nanofibers Functionalized with Reduced Graphene Oxide Nanosheets. *ACS Appl. Mater. Interfaces* **2014**, *6*, 2588–2597, doi:10.1021/am405088q.
14. Yin, L.; Chen, D.; Feng, M.; Ge, L.; Yang, D.; Song, Z.; Fan, B.; Zhang, R.; Shao, G. Hierarchical Fe<sub>2</sub>O<sub>3</sub>@WO<sub>3</sub> nanostructures with ultrahigh specific surface areas: Microwave-assisted synthesis and enhanced H<sub>2</sub>S-sensing performance. *RSC Adv.* **2015**, *5*, 328–337, doi:10.1039/C4RA10500A.
15. Deng, J.; Fu, Q.; Luo, W.; Tong, X.; Xiong, J.; Hu, Y.; Zheng, Z. Enhanced H<sub>2</sub>S gas sensing properties of undoped ZnO nanocrystalline films from QDs by low-temperature processing. *Sens. Actuators B: Chem.* **2016**, *224*, 153–158, doi:10.1016/j.snb.2015.10.022.
16. Wu, Z.; Li, Z.; Li, H.; Sun, M.; Han, Sh.; Cai, C.; Shen, W.; Fu, Y. Ultrafast Response/Recovery and High Selectivity of the H<sub>2</sub>S Gas Sensor Based on  $\alpha$ -Fe<sub>2</sub>O<sub>3</sub> Nano-Ellipsoids from One-Step Hydrothermal Synthesis. *ACS Appl. Mater. Interfaces* **2019**, *11*, 12761–12769, doi:10.1021/acsami.8b22517.
17. Wang, C.; Chu, X.; Wu, M. Detection of H<sub>2</sub>S down to ppb levels at room temperature using sensors based on ZnO nanorods. *Sens. Actuators B: Chem* **2006**, *113*, 320–323, doi:10.1016/j.snb.2005.03.011.
18. Miller, D.R.; Akbar, S.A.; Morris, P.A. Nanoscale metal oxide-based heterojunctions for gas sensing: A review. *Sens. Actuators B: Chem.* **2014**, *204*, 250–272, doi:10.1016/j.snb.2014.07.074.
19. Tai, H.; Wang, S.; Duan, Z.; Jiang, Y. Evolution of breath analysis based on humidity and gas sensors: Potential and challenges. *Sens. Actuators B: Chem.* **2020**, *318*, 128104, doi:10.1016/j.snb.2020.128104.
20. Sharma, P.K.; Ramgir, N.S.; Goyal, C.P.; Datta, N.; Srivastava, S.; Kaur, M.; Debnath, A.K.; Aswal, D.K.; Vijay, Y.K.; Gupta, S.K. Effect of sensitizers on H<sub>2</sub>S sensing properties of ZnO nanowires. In Proceedings of the International Conference on Advanced Nanomaterials & Emerging Engineering Technologies, 2013; pp. 215–217, doi:10.1109/ICANMEET.2013.6609280.
21. Zhou, X.; Lin, X.; Yang, S.; Zhu, S.; Chen, X.; Dong, B.; Bai, X.; Wen, X.; Geyu, L.; Song, H. Highly dispersed Metal–Organic–Framework–Derived Pt nanoparticles on three-dimensional macroporous ZnO for trace-level H<sub>2</sub>S sensing. *Sens. Actuators B: Chem.* **2020**, *309*, 127802, doi:10.1016/j.snb.2020.127802.
22. Wagner, R.S.; Ellis, W.C. Vapor-liquid-solid mechanism of single crystal growth. *Appl. Phys. Lett.* **1964**, *4*, 89–90, doi:10.1063/1.1753975.
23. Li, Y.; Feneberg, M.; Reiser, A.; Schirra, M.; Enchelmaier, R.; Ladenburger, A.; Langlois, A.; Sauer, R.; Thonke, K. Au-catalyzed growth processes and luminescence properties of ZnO nanopillars on Si. *J. Appl. Phys.* **2006**, *99*, 054307, doi:10.1063/1.2178395.

24. Huber, F.; Riegert, S.; Madel, M.; Thonke, K. H<sub>2</sub>S sensing in the ppb regime with zinc oxide nanowires. *Sens. Actuators B: Chem* **2017**, *239*, 358–363, doi:10.1016/j.snb.2016.08.023.
25. Pohl, H.A. *Dielectrophoresis: The Behavior of Neutral Matter in Nonuniform Electric Field*; Cambridge University Press: New York, NY, USA, 1978.
26. Siegel, J.; Lyutakov, O.; Rybka, V.; Kolská, Z.; Svorčík, V. Properties of gold nanostructures sputtered on glass. *Nanoscale Res Lett* **2011**, *6*, 96, doi:10.1186/1556-276X-6-96.
27. Kumar, R.; Al-Dossary, O.; Kumar, G.; Umar, A. Zinc Oxide Nanostructures for NO<sub>2</sub> Gas-Sensor Applications: A Review. *Nano-Micro Lett* **2015**, *7*, 97–120, doi:10.1007/s40820-014-0023-3.
28. Wu, J.; Wu, Z.; Ding, H.; Yang, X.; Wei, Y.; Xiao, M.; Yang, Z.; Wang, X. Three-Dimensional-Structured Boron- and Nitrogen-Doped Graphene Hydrogel Enabling High-Sensitivity NO<sub>2</sub> Detection at Room Temperature. *ACS Sens* **2019**, *4*, 1889–1898, doi:10.1021/acssensors.9b00769.
29. Barsan, N.; Weimar, U. Conduction model of metal oxide gas sensors. *J. Electroceramics* **2001**, *7*, 143–167.
30. Xu, J.; Wang, X.; Shen, J. Hydrothermal synthesis of In<sub>2</sub>O<sub>3</sub> for detecting H<sub>2</sub>S in air. *Sens. Actuators B: Chem* **2006**, *115*, 642–646, doi:10.1016/j.snb.2005.10.038.
31. Kim, J.; Yong, K. Mechanism study of ZnO nanorod-bundle sensors for H<sub>2</sub>S gas sensing. *J. Phys. Chem. C* **2011**, *115*, 7218–7224, doi:10.1021/jp110129f.
32. Choi, M.S.; Mirzaei, A.; Bang, J.H.; Oum, W.; Jung Kwon, Y.; Kim, J.-H.; Choi, S.-W.; Kim, S.S.; Kim, H.W. Selective H<sub>2</sub>S-sensing performance of Si nanowires through the formation of ZnO shells with Au functionalization. *Sens. Actuators B: Chem* **2019**, *289*, 1–14, doi:10.1016/j.snb.2019.03.047.
33. Michaelson, H.B. The work function of the elements and its periodicity. *J. Appl. Phys.* **1977**, *48*, 4729–4733, doi:10.1063/1.323539.
34. Choi, S.W.; Katoch, A.; Sun, G.J.; Kim, S.S. Synthesis and gas sensing performance of ZnO-SnO<sub>2</sub> nanofiber-nanowire stem-branch heterostructure. *Sens. Actuators B: Chem* **2013**, *181*, 787–794, doi:10.1016/j.snb.2013.02.010.
35. Geng, J.; Thomas, M.D.R.; Shephard, D.S.; Johnson, B.F.G. Suppressed electron hopping in a Au nanoparticle/H<sub>2</sub>S system: Development towards a H<sub>2</sub>S nanosensor. *Chem. Commun* **2005**, *14*, 1895–1897, doi:10.1039/B418559E.
36. Rai, P.; Kim, Y.S.; Song, H.M.; Song, M.K.; Yu, Y.T. The role of gold catalyst on the sensing behavior of ZnO nanorods for CO and NO<sub>2</sub> gases. *Sens. Actuators B: Chem* **2012**, *165*, 133–142. doi:10.1016/j.snb.2012.02.030.
37. Li, X.; Zhou, X.; Guo, H.; Wang, C.; Liu, J.; Sun, P.; Liu, F.; Lu, G. Design of Au@ZnO Yolk-Shell Nanospheres with Enhanced Gas Sensing Properties. *ACS Appl. Mater. Interfaces* **2014**, *6*, 18661–18667, doi:10.1021/am5057322.
38. Saito, S.; Miyayama, M.; Koumoto, K.; Yanagida, H. Gas Sensing Characteristics of Porous ZnO and Pt/ZnO Ceramics. *J. Am. Ceram. Soc.* **1985**, *68*, 40–43, doi:10.1111/j.1151-2916.1985.tb15248.x.
39. Balouria, V.; Ramgir, N.S.; Singh, A.; Debnath, A.K.; Mahajan, A.; Bedi, R.K.; Aswal, D.K.; Gupta, S.K. Enhanced H<sub>2</sub>S sensing characteristics of Au modified Fe<sub>2</sub>O<sub>3</sub> thin films. *Sens. Actuators B: Chem* **2015**, *219*, 125–132, doi:10.1016/j.snb.2015.04.113.
40. Rai, P.; Yoon, J.W.; Jeong, H.M.; Hwang, S.J.; Kwak, C.H.; Lee, J.H. Design of highly sensitive and selective Au@NiO yolk-shell nanoreactors for gas sensor applications. *Nanoscale* **2014**, *6*, 8292–8299, doi:10.1039/C4NR01906G.

**Publisher's Note:** MDPI stays neutral with regard to jurisdictional claims in published maps and institutional affiliations.



© 2020 by the authors. Submitted for possible open access publication under the terms and conditions of the Creative Commons Attribution (CC BY) license (<http://creativecommons.org/licenses/by/4.0/>).